JOURNAL OF AIRCRAFT
Vol. 29, No. 6, Nov.–Dec. 1992

Wind-Tunnel Investigation of a Fighter Model at High Angles of Attack

Sheshagiri K. Hebbar* and David H. Leedy†
Naval Postgraduate School, Monterey, California 93943

A low-speed wind-tunnel investigation was conducted to examine the aerodynamic characteristics of the flowfield around a 3% scale model of YF-17 lightweight fighter prototype at high angles of attack using laser sheet flow visualization and force and moment measurements. The data indicate a good correlation between the observed flow phenomena and force and moment measurements at various orientations of the model, thus establishing the credibility of such experimental investigations for high-angle-of-attack aerodynamic research. The asymmetric shedding of vortices generated by the slender nose and leading-edge extensions (strakes) of the model dominate the aerodynamic phenomenon between 45- and 65-deg angle of attack. The roll and yaw angles have considerable influence on vortex development and consequently on flow behavior at high angles of attack.

Introduction

EXPANDING the maneuvering envelope boundaries of a tactical aircraft to include controlled flight in the low-speed, high-angle-of-attack regime is a primary concern of today's aircraft designers. Studies have shown that the ability to perform rapid, transient maneuvers, even into poststall flight, can greatly enhance an aircraft's air combat capability and significantly improve mission success. These capabilities are highly dependent upon maintaining a high degree of control effectiveness throughout the maneuvering angle-of-attack range and about all aircraft axes.[1]

Though not designed for supermaneuverability, many recently developed aircraft have achieved improved high-angle-of-attack performance by incorporating innovative aerodynamic design features. The Northrop Corporation developed the hybrid wing concept in the late 1960's and applied it to the YF-17 lightweight fighter prototype in 1972 in direct response to the challenge of achieving maximum lift and angle of attack, while maintaining positive stability and control. The hybrid wing planform of the YF-17 results from the combining of a conventional wing with moderate sweepback and aspect ratio, with a wing root leading-edge extension (LEX), also known as a strake. The LEX induces a vortex flow which increases in strength with increasing angle of attack. The stable vortex flow creates an area of high negative pressure on the upper surface of the wing that increases lift and delays separation to much higher angles of attack than would be possible with conventional wing alone. The flight envelope of the aircraft is expanded by the improved stability and control of the aircraft in the high-angle-of-attack regime.[2]

The separation of flow from the body of an aircraft exerts considerable aerodynamic forces that must be understood and controlled if true supermaneuverability is to be realized in our next generation of tactical aircraft. The high-angle-of-attack characteristics of a fighter aircraft are highly configuration dependent[1] and vortex dominated. The yaw control provided by a conventional rudder decreases with increasing angle of attack as the tail becomes blanketed by the stalled flow from the wing. Reduced maneuvering capability results from inadequate yaw control just when maximum rudder effectiveness is required. The long slender nose of a modern fighter aircraft also contributes to this problem by producing powerful vortex flowfields at high angles of attack. The side forces generated by the asymmetric shedding of these vortices coupled with the long moment arm from the nose to the aircraft's center of gravity present a control problem of significant proportion.[1,3]

This investigation was undertaken at the Naval Postgraduate School (NPS), to characterize the flowfield around a fighter aircraft model, specifically, the YF-17.[4,5] It should be emphasized that the intent of this investigation was to gain insight into the high-angle-of-attack behavior of a current fighter aircraft as a whole, not just concentrating on the effects of singular concepts at work in the design such as the hybrid wing. In addition to extensive laser sheet flow visualization data, measurements were made to obtain force and moment data on the model and the correlation between these two sets examined to provide insight into areas of aerodynamic interest in the flowfield.

Experiment

The experimental setup is described below briefly. More details may be found in Refs. 4 and 5.

Test Configuration

Experimental investigations were carried out in the NPS low-speed wind-tunnel facility which is of single-return-type powered by a 100 horsepower electric motor coupled to a three-bladed variable pitch fan by way of a four-speed transmission. The tunnel has a contraction ratio of 10:1, a test section of 1.143 × 0.813 m, and a nominal freestream turbulence level of 0.2%. The test section has hinged glass windows on either side for easy access and unobstructed viewing. A remotely controlled horizontal turntable located in the center of the test section floor allows for model mounting and variable pitch angles. The fighter model (on loan from Northrop Corporation) used is a 3% scale model of the Northrop Corporation's YF-17 lightweight fighter prototype (Fig. 1) made of steel and aluminum. It has a wing span of 32 cm, a mean aerodynamic chord of 9.85 cm, and a wing area of 292.6 cm^2. The balance block section of the model accommodates a 25.4-mm-diam 6-component strain-gauge-type precision balance (on loan from NASA-Ames Research Center) made by Task Corporation.

The model is held in the test section in a vertical plane (right wing down) supported by the balance which is connected to a balance support or sting (Fig. 2). The sting extends aft of the model and fits securely with a rigid vertical swinging

Presented as Paper 90-3019 at the AIAA 8th Applied Aerodynamics Conference, Portland, OR, Aug. 20–22, 1990; received Jan. 26, 1991; revision received Dec. 3, 1991; accepted for publication Dec. 3, 1991.

*Adjunct Professor, Department of Aeronautics and Astronautics. Associate Fellow AIAA.
†Commander, United States Navy.

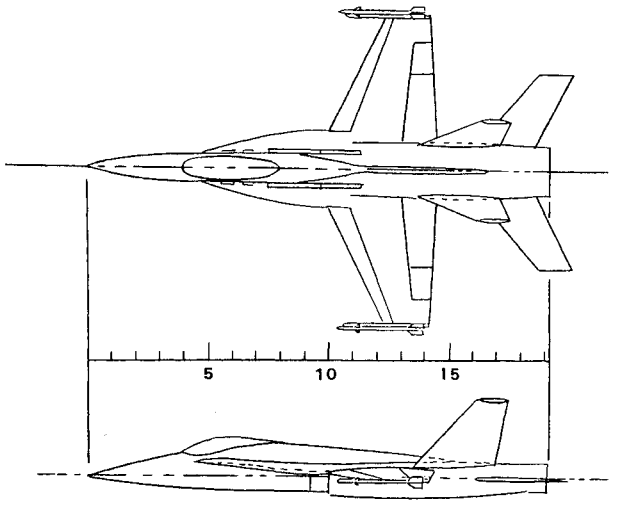

Fig. 1 Three percent scale model of YF-17 fighter prototype.

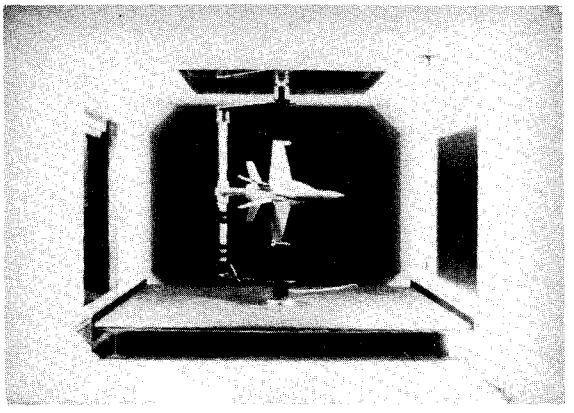

Fig. 2 YF-17 fighter model sting-mounted in the test section of the NPS wind tunnel (view from the settling chamber).

arm assembly which is securely fixed to the turntable at the base and supported by a 25.4-mm steel pin through the 19-mm-thick Plexiglas® viewing window on top. The sting mount and swinging arm assembly permit pitch angles (α) of -35 to $+90$ deg, yaw angles (β) of ± 5, ± 10, or ± 15 deg, and 360-deg roll (ϕ). The arm assembly pivot point, model center of pressure, and balance center all coincide. Note that the model is pitched in the horizontal plane and yawed in the vertical plane.

Data Acquisition System

A signal conditioning circuit for each individual strain gauge in the balance supplies voltage for calibration and zeroing. The signal conditioner output is fed to a Hewlett-Packard relay multiplexer which sequentially cycles through each balance channel as specified by a data acquisition program. A 1000 gain, low-noise amplifier boosts the output signal to improve the resolution after which the analog voltage signal is converted to a digital signal by a HP digital multimeter for use in the software program. An IBM-AT microcomputer controls data acquisition and model positioning during the experiment and stores the collected data. The data acquisition program controls the HP instrument package and transforms each balance channel's output into a compatible format. The balance readings are time-averaged, combined with appropriate calibration constants and then converted to coefficient form for ease of data comparison, taking into account the test conditions and model blockage. Details of correction for model blockage are given in Ref. 4.

Flow Visualization System

Details of the flow visualization system using smoke and a laser sheet for illumination are available in Refs. 4, 6, and 7. A special feature of this system is the use of fiber optics to transport the laser beam in a safe and convenient manner. Major components of the system include a portable smoke generating machine, a portable 25.4-mm smoke tube, a 5-W Argon-ion laser, and associated optics mounted on a traverse mechanism to permit complete coverage of the wind-tunnel test section. The thickness of the laser sheet is approximately 2 mm.

Test Conditions

The experiment was carried out in two phases. The first phase involved the measurement of forces and moments on the model for angles of attack varying from -35 to $+85$ deg at a tunnel velocity of 50 m/s, corresponding to a Reynolds number of 3.49×10^5 (based on model mean aerodynamic chord). In the second phase, extensive laser sheet visualization of the model flowfield was accomplished at a tunnel velocity of 10 m/s. Both videotape recording and cross-sectional photography of the flowfield over the model were performed to identify the areas most likely affected by vortex generation and separation.

Results and Discussion

The results of the investigation are presented and discussed in some detail in two parts. First, the flow visualization data will be analyzed and then the force and moment data examined. More detailed analysis/examination of these data and their correlation appears in Ref. 4.

Flow Visualization Data

The model attitude was varied between 0–45 deg of roll, and 0–15 deg of yaw. The majority of flow visualization photography was performed between 20–70 deg of pitch. In Ref. 4 the results of the 35-mm photography are presented and discussed in a series of photographic sequences depending on aircraft orientation in three categories, namely, pitch only, pitch and roll, and pitch and yaw. Here some typical photographs will be presented and examined in some detail to identify the dominant flow phenomena in different orientations. Table 1 lists some prominent stations and model features at these locations. "Station" refers to the number of inches aft of the nose at which the laser sheet cuts the longitudinal axis perpendicularly. The scaling in Fig. 1 provides a visual reference to these stations and aids discussion of the flow visualization data.

The effect of pitch on and the downstream development of forebody vortices on the YF-17 model in the absence of roll and yaw have been examined in Ref. 4 and are in good agreement with the asymmetric vortex flow behavior that has been well documented in the literature for slender nose bodies at high angles of attack.[8] Figures 3–6 show the effect of roll on forebody vortices at station 1 with the pitch angle held constant at 65 deg. Comparison of Fig. 4 with Fig. 3 shows little change in the orientation of the two vortices other than a slight separation of the bottom vortex from the nose surface. Figure 5 shows the development of a significant separation of the bottom vortex which increases as the model is rolled to 45 deg in Fig. 6. The nose geometry of the YF-17 is a major factor in this phenomenon.

Table 1 Station identification on the model

Station	Description (see Fig. 1)
0	Tip of nose
4	Forwardmost edge of canopy
5.25	Beginning of leading-edge extension (LEX) or strake
10	Intersection of LEX and wing leading edge
12	Model c.p.; balance center point
14	Intersection of leading edge of vertical stabilizers and fuselage
14.5	Trailing edge of wings

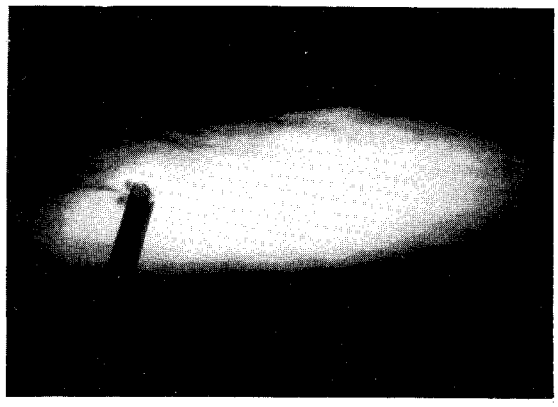

Fig. 3 Forebody vortices at station 1, α = 65 deg, β = 0 deg, ϕ = 0 deg.

Fig. 4 Forebody vortices at station 1, α = 65 deg, β = 0 deg, ϕ = 15 deg.

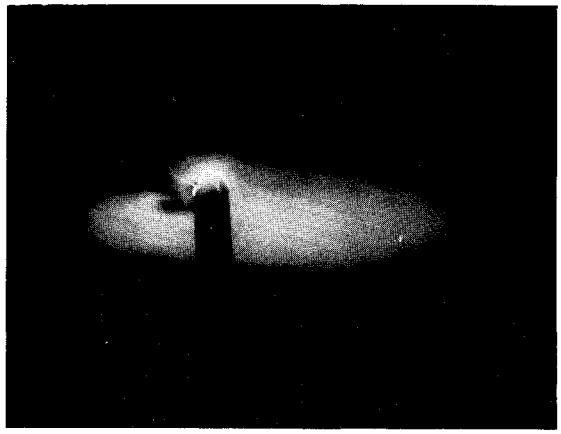

Fig. 5 Forebody vortices at station 1, α = 65 deg, β = 0 deg, ϕ = 30 deg.

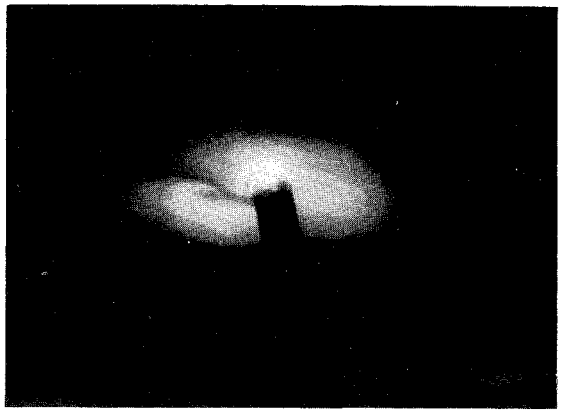

Fig. 6 Forebody vortices at station 1, α = 65 deg, β = 0 deg, ϕ = 45 deg.

The effect of roll on the strake (LEX) generated vortices shows up dramatically in the sequence of photographs Figs. 7–9, where the laser sheet has been positioned at station 8 and the model roll angle increased from 15 to 45 deg at a constant angle of attack of 55 deg. No strake vortices are seen in Fig. 7; they are already burst at this model orientation (high relative angle of attack) and the flow is completely separated and turbulent. But with further increase in the roll angle, the strake generated vortex on the downwind side (right side) of the fuselage gains strength as can be seen by the tightening of the flow and improved definition of the (bottom) vortex core. The reduction in the relative angle of attack on the downwind strake with increasing roll is primarily responsible for this vortex enhancement. As a matter of fact the flow goes from completely turbulent in Fig. 7 to asymmetric and semiattached at 45-deg roll in Fig. 9.

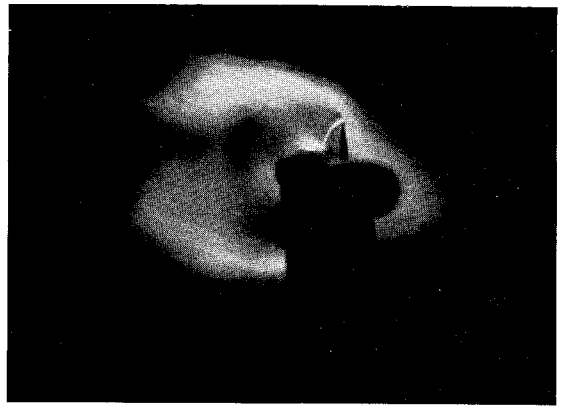

Fig. 7 Strake (LEX) vortices at station 8, α = 55 deg, β = 0 deg, ϕ = 15 deg.

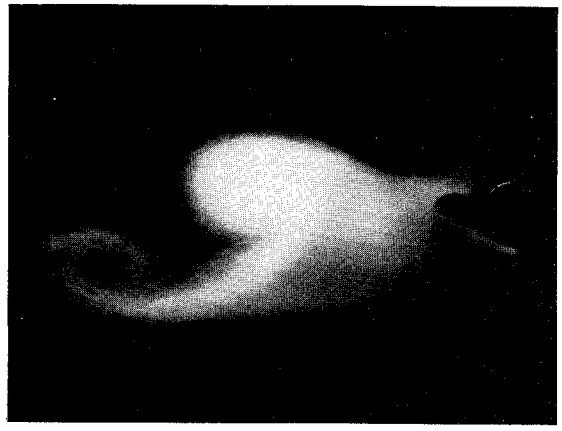

Fig. 8 Strake (LEX) vortices at station 8, α = 55 deg, β = 0 deg, ϕ = 30 deg.

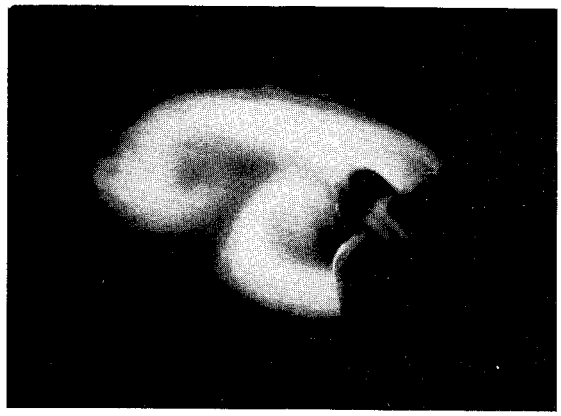

Fig. 9 Strake (LEX) vortices at station 8, α = 55 deg, β = 0 deg, ϕ = 45 deg.

The disappearance of the upwind strake generated vortex and the stability of the downwind strake generated vortex are documented in the sequence of photographs (Figs. 10–13) taken at station 10 with the model angle of attack increasing from 25 to 40 deg and the roll and yaw angles held constant at 30 and 0 deg, respectively. Note that station 10 is the point on the fuselage where the leading edge of the wing meets the leading edge of the LEX. At 25-deg angle of attack, the strake generated vortices are visible on both sides of the fuselage. The left side or upwind vortex (top vortex in Fig. 10) is slightly larger, indicating less strength and stability. This is predictable given the higher relative angle of attack on that side. Increasing the angle of attack to 30 deg causes the left side vortex to burst while the right side or downwind vortex (bottom vortex in Fig. 11) weakens slightly but remains intact. Figures 12 and 13 complete the sequence.

Fig. 10 Strake (LEX) vortices at station 10, α = 25 deg, β = 0 deg, ϕ = 30 deg.

Fig. 11 Strake (LEX) vortices at station 10, α = 30 deg, β = 0 deg, ϕ = 30 deg.

Fig. 12 Strake (LEX) vortices at station 10, α = 35 deg, β = 0 deg, ϕ = 30 deg.

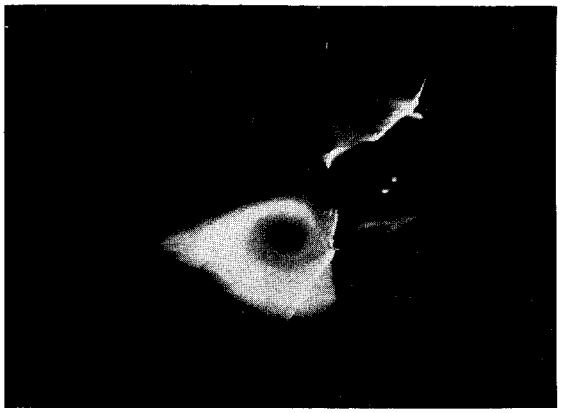

Fig. 13 Strake (LEX) vortices at station 10, α = 40 deg, β = 0 deg, ϕ = 30 deg.

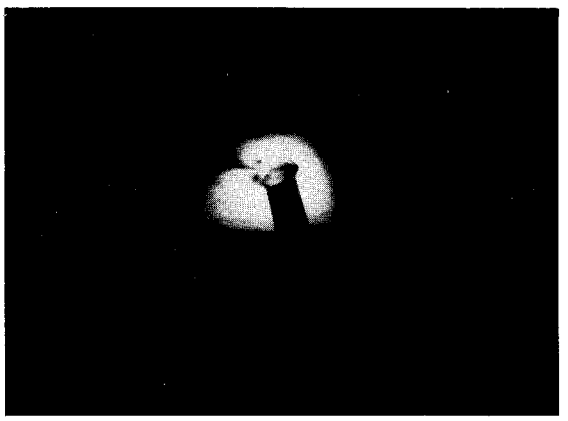

Fig. 14 Forebody vortices at station 1, α = 50 deg, β = 5 deg, ϕ = 0 deg.

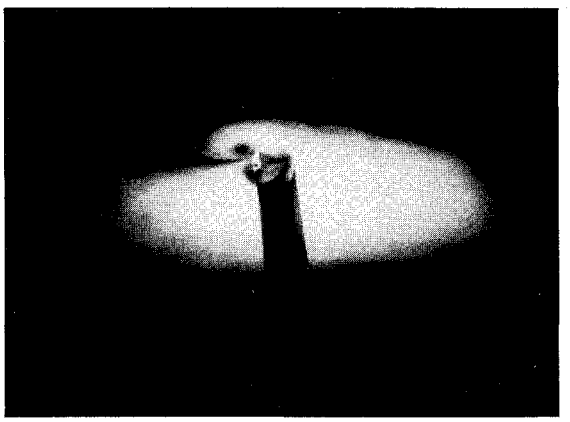

Fig. 15 Forebody vortices at station 1, α = 65 deg, β = 5 deg, ϕ = 0 deg.

The effect of yaw is illustrated in Figs. 14 and 15 which highlight the difference in the formation of nose generated vortices at station 1 when the 5 deg yawed model was pitched from 50- to 65-deg angle of attack. The vortices in Fig. 14 are nicely formed and are nearly symmetric, but have already begun to go asymmetric in Fig. 15. It must be noted here that the flow visualization tests indicated some unsteadiness of the forebody generated vortices at the lower angle of attack (50 deg). Both vortices remained attached, but never in the same place for very long. A comparison of the orientations of the vortex cores in the photographs taken less than 2 s apart clearly revealed the unsteadiness (see Refs. 6 and 7). However, there was no evidence of vortex unsteadiness at the higher angle of attack (65 deg).

The bursting of the left side (or upwind) wing vortex is traced from station 10 to station 14.5 in the sequence of pho-

tographs, Figs. 16–19, at an angle of attack of 25 deg, yaw of 5 deg and roll of 0 deg. The upwind wing vortex is easily identifiable in Fig. 16. The bursting of the vortex and the consequent loss of vortex coherence are clearly seen in Figs. 17 and 18. In Fig. 19, the vertical tail is immersed in completely turbulent flow which has proven, in other investigations, to be a major factor in reducing the fatigue life of the tail structures.

Force and Moment Data

A few comments about the expected errors in the measurements are in order. Factors beyond experimental control, such as slight voltage fluctuations in the power supply (which in turn caused drift and variation in the measurement of forces and moments) and the inability to establish exact pitch attitudes, consistently led to some variation in the data from run

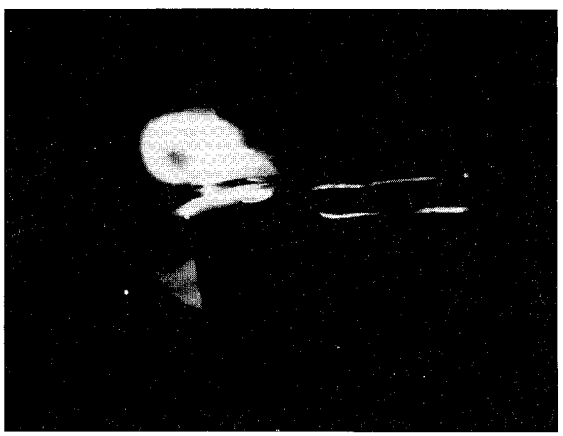

Fig. 16 Upwind wing vortex at station 10, α = 25 deg, β = 5 deg, ϕ = 0 deg.

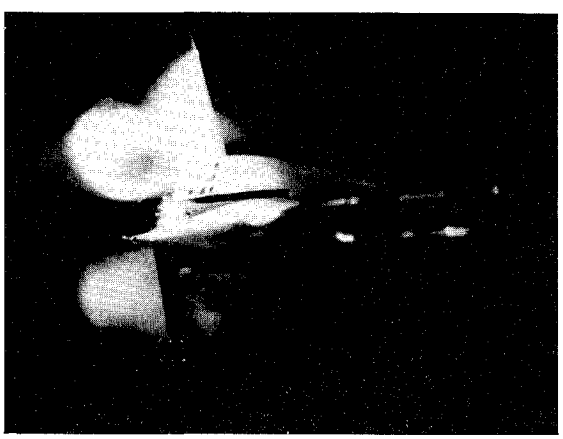

Fig. 17 Upwind wing vortex at station 11, α = 25 deg, β = 5 deg, ϕ = 0 deg.

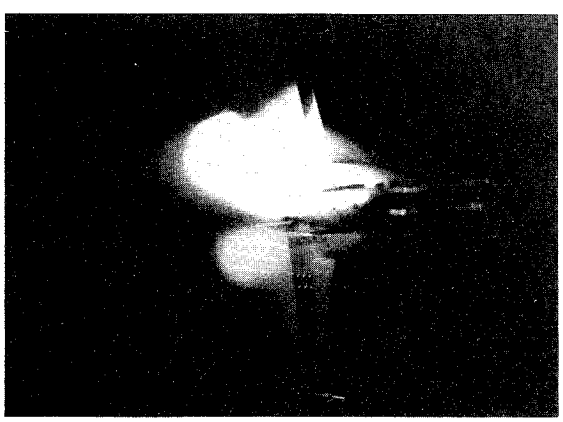

Fig. 18 Upwind wing vortex at station 13, α = 25 deg, β = 5 deg, ϕ = 0 deg.

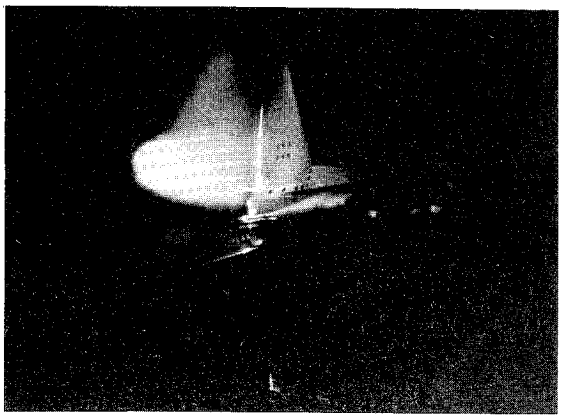

Fig. 19 Upwind wing vortex at station 14.5, α = 25 deg, β = 5 deg, ϕ = 0 deg.

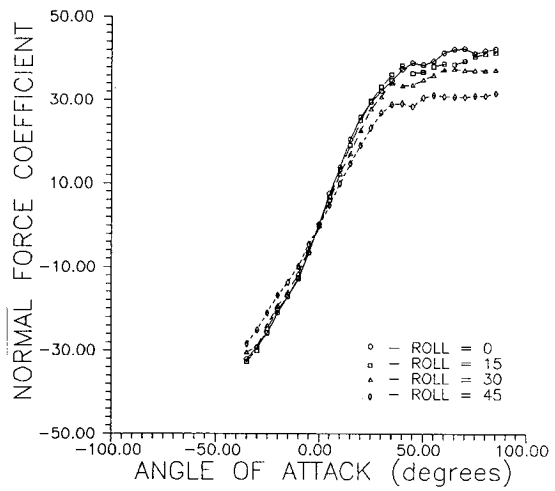

Fig. 20 Normal force coefficient as a function of angle of attack for different roll angles at zero yaw.

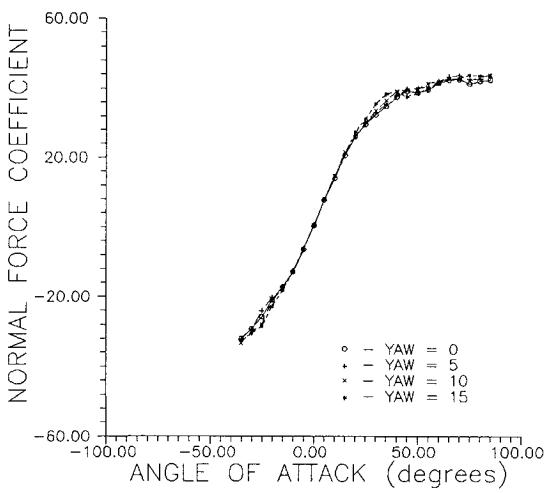

Fig. 21 Normal force coefficient as a function of angle of attack for different yaw angles at zero roll.

to run. The desired angles of attack were multiples of 5 deg, but the actual angle of attack established varied by as much as ±0.5 deg from the target angle of attack. In the case of the normal force, data repeatability was excellent with an expected maximum variation in the order of 1.33 N (0.3 lb) observed near 35–40-deg angle-of-attack range. The expected variations for the side force and moments were in the order of 2.22 N (0.5 lb) and 0.14 N·m (0.1 ft-lb), respectively.

The normal force coefficient plots in Figs. 20 and 21 show a characteristic rise with increasing angle of attack to a max-

imum value, after which the magnitude attains a near steady value though the angle of attack continues to rise. Figure 20 shows separate curves for each roll angle (at zero yaw angle). The normal force coefficient plots are nearly equal through 30-deg angle-of-attack range where they start to level and separate. At this point, the roll angle and the normal force coefficient become inversely proportional with the highest roll angle experiencing the lowest normal force. This makes perfect sense in that the higher roll angle configuration presents less surface area to the flow. Leveling of the normal force coefficient curves can be correlated to the transition of the flow over the model from vortex flow to separated wake-like flow observed in the flow visualization data at high angles of attack (see Ref. 4 for details of correlation). The plots of Fig. 21 corresponding to four different yaw angles at zero roll angle are nearly identical due to the unchanged planform area, and provide a degree of confidence in the balance readings given the time separation between data collection for each angle. The curves exhibit the same leveling tendency as the zero degree roll angle curve in Fig. 20 for exactly the same reasons.

The side force coefficient plots in Figs. 22 and 23 contain data which can be correlated to the observed flow phenomena present at certain angles of attack, roll, and yaw. Each curve in Fig. 22 represents a different roll angle (at zero yaw). At 0-deg angle of attack, the side force coefficients for each curve intersect at zero. The side force coefficient magnitude generally increases with increasing pitch and roll to a point where the magnitude levels off except in the case of 0 deg roll. The peak in the curve for 0 deg roll between 45–65-deg angle of attack corresponds to a region of active nose vortices. The asymmetric shedding of these vortices[4,5] is responsible for the variation in side force coefficients evident in the curve. Although the same type of shedding vortex behavior is seen for all roll angles (see photographic sequences 3–12 in Ref. 4), the curves for roll angles greater than 0 deg do not clearly define the areas of increased side force due to the shedding vortices because of the off-setting effect of the crossflow component of the freestream velocity. The shedding vortices are active but somewhat negated.

Figure 23 depicts side force coefficients as a function of the angle of attack for four different yaw angles (at zero roll angle). In the vicinity of 0-deg angle of attack, all curves for yaw angles greater than zero exhibit rise in magnitude in response to the crossflow component of the relative wind. All the curves show the same characteristic peak between 45–65-deg angle of attack, though the curves corresponding to positive yaw angles peak to a lesser degree than the curve for 0 deg yaw. Maximum asymmetric vortex activity was identified during flow visualization in this angle-of-attack range and unquestionably accounts for the side force fluctuations present in the coefficient plots (see photographic sequence 30 in Ref. 4).

Figures 24 and 25 present the rolling moment coefficient data for different roll angles and yaw angles, respectively. The peak seen in Fig. 24 between 30–60-deg angle of attack is a result of the asymmetry between the LEX generated vortices on either side of the fuselage. The supporting pho-

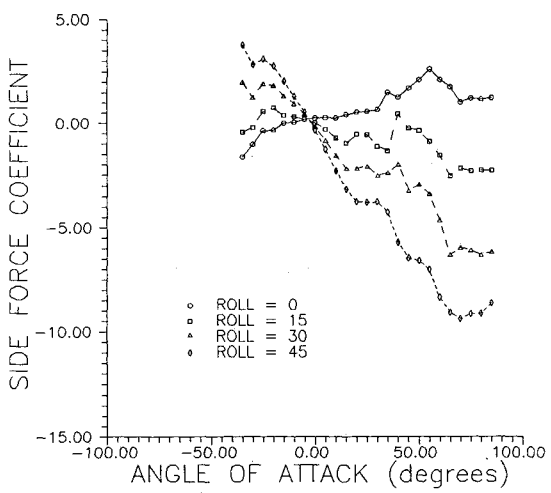

Fig. 22 Side force coefficient as a function of angle of attack for different roll angles at zero yaw.

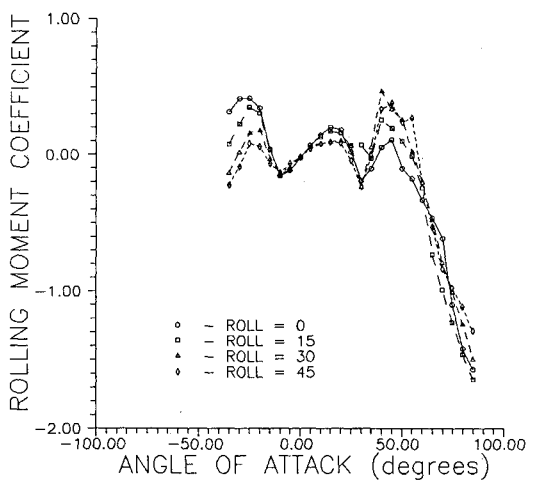

Fig. 24 Rolling moment coefficient as a function of angle of attack for different roll angles at zero yaw.

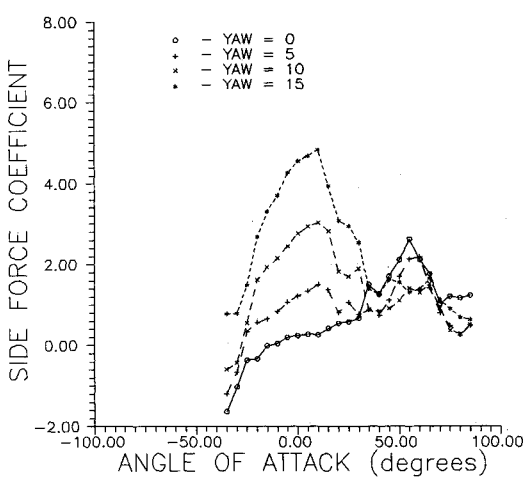

Fig. 23 Side force coefficient as a function of angle of attack for different yaw angles at zero roll.

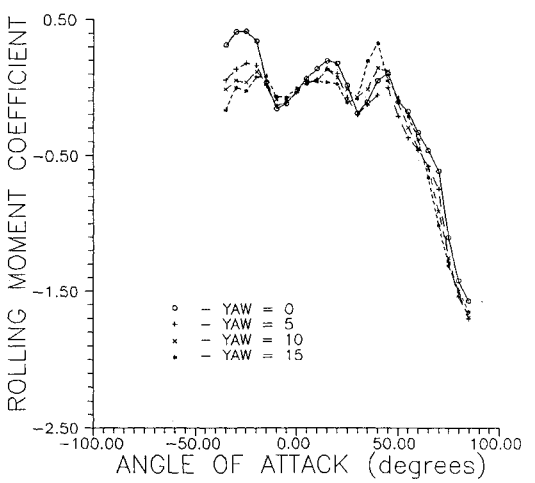

Fig. 25 Rolling moment coefficient as a function of angle of attack for different yaw angles at zero roll.

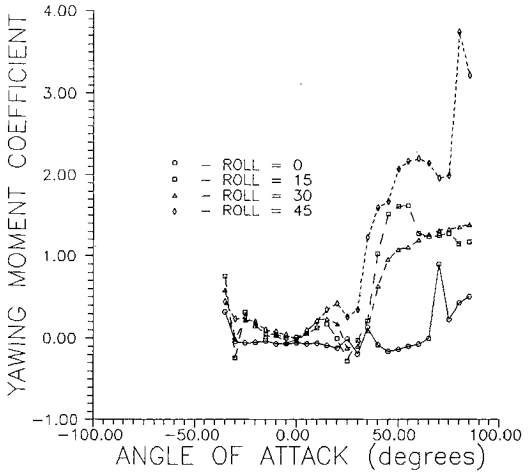

Fig. 26 Yawing moment coefficient as a function of angle of attack for different roll angles at zero yaw.

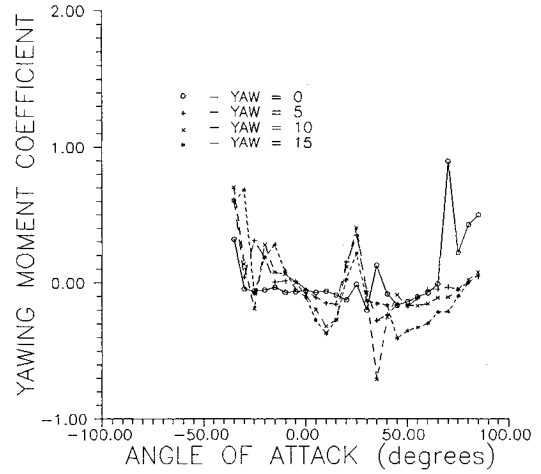

Fig. 27 Yawing moment coefficient as a function of angle of attack for different yaw angles at zero roll.

tographic evidence (see photographic sequences 14–19 in Ref. 4) indicates that the largest magnitude of rolling moment coefficient should correspond to an angle of attack of 45 deg and a roll angle of 45 deg. The maximum rolling moment coefficient in Fig. 24 reflects this observation. Note that the minimum rolling moment coefficient in the same angle-of-attack range occurs for the 0-deg roll curve, as this is the model attitude which generates the least asymmetry between the LEX generated vortices. Figure 25 also shows a peak in the 30–50-deg angle-of-attack range, the greatest magnitude of rolling moment coefficient occurring for a yaw angle of 15 deg which is the model attitude generating the greatest asymmetry between the LEX generated vortices in the yaw-only test configuration.

Figures 26 and 27 show the yawing moment coefficient data for different roll angles and yaw angles, respectively. Both figures present data which cannot be easily correlated with the flow visualization data. The data in Fig. 26 appears to be responding mostly to the side forces generated by crossflow. The two large magnitude fluctuations seen at 70- and 80-deg angle of attack for the 0 and 45 deg roll test configurations, respectively, do not readily correspond with any of the observed flow phenomena. In addition, the large fluctuations seen in the curve in Fig. 27 between 0- and 45-deg angle of attack were not expected. The large yawing moments would have seemed more likely to occur near the 50–55-deg angle-of-attack range where the greatest unsteadiness in the flow was visually recorded during flow visualization experiments. It is suspected that the data acquisition system was too slow to accurately reflect changes in yawing moment.

Conclusions

A low-speed wind-tunnel investigation was conducted into the high-angle-of-attack aerodynamics of a 3% scale YF-17 lightweight fighter prototype model using flow visualization and balance measurements, to identify flow phenomena that may prove important in the design and performance of supermaneuverable aircraft. The following conclusions are drawn from the results of the experimental investigation:

1) A good correlation between the observed flow phenomena and force and moment measurements existed between 25–70 deg angle of attack. Maximum side forces and yawing moments are observed when the strake (LEX) and nose generated vortices are strongest.

2) The predominant aerodynamic phenomenon between 45–65-deg angle of attack is the asymmetric shedding of vortices generated by the slender nose and leading-edge extensions (strakes) of the model. Maximum side forces are generated in this angle-of-attack range.

3) Below 45-deg angle of attack, the flow characteristics are governed by complex multiple vortex interactions along the upper surface of the fuselage and wings coupled with nose generated vortices.

4) The roll and yaw angles are major factors in flow behavior at high angles of attack.

Acknowledgment

The authors owe a deep debt of gratitude to the late S. Bodapati for initiating this investigation. The authors sincerely thank M. Platzer for his encouragement and suggestions during the investigation. This work which formed the M.S. thesis of one of the authors (DHL) was sponsored by the Naval Air Systems Command and the Naval Postgraduate School.

References

[1]Murri, D. G., and Rao, D. M., "Exploratory Studies of Actuated Forebody Strakes for Yaw Control at High Angles of Attack," AIAA Paper 87-2557, Aug. 1987.

[2]Patierno, J., "Evolution of the Hybrid Wing-YF-17/F-18 Type," *Proceedings of the AIAA Symposium on Evolution of Aircraft Wing Design*, Dayton, OH, March 1980, pp. 131–139.

[3]Webster, F. R., "High Angle of Attack Flight Tests of the F-15C," AFFTC-TR-83-33, Edwards AFB, CA, Oct. 1983.

[4]Leedy, D. H., "An Experimental Investigation of a Fighter Aircraft Model at High Angles of Attack," M.S. Thesis, Naval Postgraduate School, Monterey, CA, Sept. 1988.

[5]Hebbar, S. K., and Leedy, D. H., "A Laser Sheet Flow Visualization and Aerodynamic Force Data Evaluation of a 3% YF-17 Fighter Aircraft Model at High Angles of Attack," AIAA Paper 90-3019, 1990.

[6]Chlebanowski, J. S., "Flow Visualization by Laser Sheet," M.S. Thesis, Naval Postgraduate School, Monterey, CA, March 1988.

[7]Hebbar, S. K., Chandrasekhara, M. S., and Chlebanowski, J. S., "Flow Visualization by Laser Sheet," Fourth Asian Congress of Fluid Mechanics, Hong Kong, Aug. 21–25, 1989.

[8]Chapman, G. T., and Keener, E. R., "The Aerodynamics of Bodies of Revolution at Angles of Attack to 90 Degrees," AIAA Paper 79-0023, 1979.